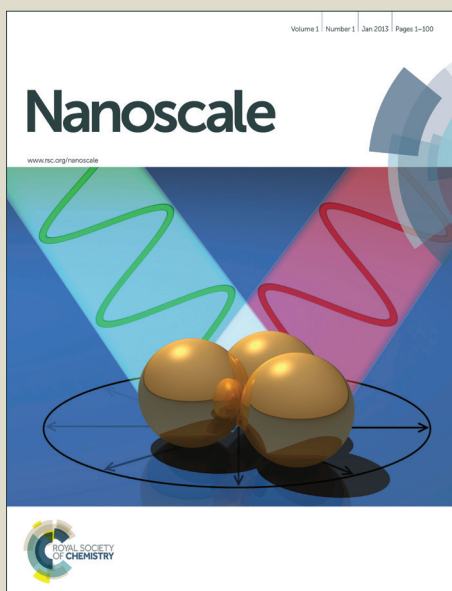


Nanoscale

Accepted Manuscript



This is an *Accepted Manuscript*, which has been through the Royal Society of Chemistry peer review process and has been accepted for publication.

Accepted Manuscripts are published online shortly after acceptance, before technical editing, formatting and proof reading. Using this free service, authors can make their results available to the community, in citable form, before we publish the edited article. We will replace this *Accepted Manuscript* with the edited and formatted *Advance Article* as soon as it is available.

You can find more information about *Accepted Manuscripts* in the [Information for Authors](#).

Please note that technical editing may introduce minor changes to the text and/or graphics, which may alter content. The journal's standard [Terms & Conditions](#) and the [Ethical guidelines](#) still apply. In no event shall the Royal Society of Chemistry be held responsible for any errors or omissions in this *Accepted Manuscript* or any consequences arising from the use of any information it contains.

Cite this: DOI: 10.1039/c0xx00000x

www.rsc.org/xxxxxx

ARTICLE TYPE

Controlled assembly and single electron charging of monolayer protected Au₁₄₄ clusters: electrochemistry and scanning tunneling spectroscopy study

Nataraju Bodappa^a, Ulrike Fluch^b, Yongchun Fu^{*a}, Marcel Mayor^{*b,c}, Pavel Moreno-García^a, Hans Siegenthaler^a and Thomas Wandlowski^a

Received (in XXX, XXX) Xth XXXXXXXXXX 20XX, Accepted Xth XXXXXXXXXX 20XX

DOI: 10.1039/b000000x

Single gold particles may serve as room temperature single electron memory units due to their size dependent electronic level spacing. Here we present a proof of concept study by electrochemically controlled scanning probe experiments performed on tailor-made Au particles of narrow dispersity. In particular the charge transport characteristics through chemically synthesized hexane-1-thiol and 4-pyridylbenzene-1-thiol mixed monolayer protected Au₁₄₄ clusters (MPCs) by differential pulse voltammetry (DPV) and electrochemical scanning tunneling spectroscopy (EC-STs) are reported. The pyridyl groups exposed by the Au-MPCs enable their immobilization on Pt(111) substrates. By varying the humidity during their deposition, samples coated by stacks of compact monolayers of Au-MPCs or decorated with individual, laterally separated Au-MPCs are obtained. DPV experiments with stacked monolayers of Au₁₄₄-MPCs and EC-STs experiments with laterally separated individual Au₁₄₄-MPCs are performed both in aqueous and ionic liquid electrolytes. Lower capacitance values were observed for individual clusters compared to ensemble clusters. This trend remains the same irrespective of the composition of the electrolyte surrounding to the Au₁₄₄-MPC. The resolution of the energy level spacing of single clusters however, is strongly affected by the proximity of neighboring particles.

Nanoscale Accepted Manuscript

Cite this: DOI: 10.1039/c0xx00000x

www.rsc.org/xxxxxx

ARTICLE TYPE

1. Introduction

The miniaturization trend of electronic circuits is focusing on new materials and methods to fabricate devices with feature sizes in the scale below the state-of-art of the current CMOS technique.¹ Most of these devices described in the literature are based on metal or semiconductor nanoparticles (NPs) and are mainly conceptual demonstrators working at low temperatures²⁻⁵ and in vacuum.^{6, 7} Nanoelectronic devices operating at a single electron level in ambient environment and at room temperature require rigorous control over the atomic scale dimensions and interactions of their building blocks,⁸ involving very small components with precise dimensional control. Objects in a suitable size range are large aromatic molecules or NPs with diameters below 5 nm. Aromatic molecular systems have recently received great attention due to their well defined structure for the exploration of a series of single molecule based transistors and switches.⁹

A very interesting pathway is based on monolayer-protected gold clusters (Au MPCs) coated with thiols, phosphenes or acetylenes as protecting ligands. The syntheses of these Au MPCs have been extensively studied and improved to almost atomic scale precision in the last decade.¹⁰ As these particles have a size of less than 2 nm, they fulfill all the required conditions to observe single electron charging phenomena at room temperature.^{11, 12} They have also been suggested to be suitable systems for the fabrication of single electron transistors,^{7, 13-15} switches,^{16, 17} sensors,^{18, 19} symmetric metal-insulator-NP-insulator-metal capacitors²⁰ and charge trap memory devices.^{21, 22} However, only a few studies have been reported on their practical applications at ambient temperature.^{15, 23-28} Due to the property of quantized charging at room temperature, Au MPCs can be used to manipulate the electronic function in integrated electronic circuits at the single electron level.¹² This feature of Au MPCs is particularly appealing as it provides the required digital information triggered on a single electron level. Electrochemical techniques play a crucial role in understanding many aspects of Au MPCs,^{12, 29-31} such as their charging behavior, size dispersion, HOMO-LUMO gap and electron transfer kinetics. However, conventional electrochemical techniques are limited to the study of Au MPC ensembles, and therefore probe only their average response. To understand the electron transport through the individual Au MPCs in electrical circuits, electrochemical scanning tunneling microscopy (STM) combined with spectroscopic (STS) techniques appears to be a useful method. These techniques provide insight into the tunneling current characteristics of a single NP enclosed between the STM tip and the substrate. Recently, redox mediated single molecule-based transistors³²⁻³⁸ and switches³⁹⁻⁴² were explored with these techniques by several research groups. On the other hand, to manipulate the charging of an Au₁₄₄ cluster device, the concept of electrochemical gating was introduced.²⁶

The practical application of aqueous electrolytes in previous studies²⁶ is limited to ambient or lower temperatures due to their relatively high volatility. In experiments requiring elevated temperature a highly stable and non-volatile environment is desired. These boundary conditions are perfectly matched by

room temperature ionic liquids (RTILs). Their high thermal stability, non-volatility, as well as a considerably broader potential window (often exceeding 4–5 V) of RTILs compared to the aqueous environment enables to access more charging states in a wide temperature range. However, their real accessible potential/temperature window is still restricted by the residue water, which is difficult to be removed completely. These favorable features considerably improve the application potential with respect to future nanoelectronic devices based on single-electron redox switching. Inspired by this, we have addressed quantized double-layer charging dynamics of hexanethiolate protected Au₁₄₄ clusters in various hydrophobic RTILs.^{43, 44}

In the nanometer scale, most of the electronic properties of NPs are very sensitive to inter-particle interactions. In the case of semiconductor NPs, it has been shown that interparticle interactions are quite significant for their local electronic properties.^{45,}

However, to the best of our knowledge, the observation of neighboring particle effects upon local electronic properties is quite limited in the case of metal NPs. Over the past years, NP assemblies moved into the focus of interest⁴⁷ due to the diversity of their possible applications in electronics, magnetism, optics, and catalysis. Improved handling and control of NP assemblies is also of benefit for the integration of NPs into electrical circuits.

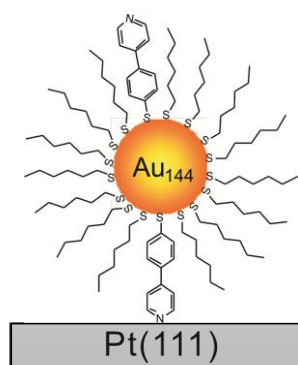


Fig. 1 Schematic of the hexane-1-thiol and 4-pyridylbenzene-1-thiol monolayer protected Au₁₄₄ clusters (Au₁₄₄ MPCs) assembled on Pt(111) surface.

In this work, we present the controlled assembly of tailor-made monolayer protected Au₁₄₄ clusters (Au₁₄₄ MPCs) which are mainly protected by hexylthiolates, but comprise also a few 4-(pyridin-4'-yl)benzenethiolates to immobilize the Au₁₄₄ cluster on a Pt(111) substrate (**Fig. 1**). Depending on the assembly conditions, the Au₁₄₄ MPC coverage ranges from stacks of several densely packed monolayers to individual clusters in sub-monolayers. We have subsequently investigated the electronic properties of Au₁₄₄ MPCs by differential pulse voltammetry (DPV) and scanning tunneling spectroscopy (STS) in three different types of electrolytes: An organic solvent (0.01 M BTTPA-TPFB, bis(triphenylphosphoranylidene) ammonium tetrakis(penta-fluorophenyl)borate/CH₃CN), an aqueous electrolyte (0.1 M NaClO₄), and a RTIL, [C₆C₁Im][FEP]. Thereby we are not only able to demonstrate single electron switching at room temperature, but also to establish the influence of the immediate proximity of the Au₁₄₄ MPC on its electronic features. In addition, we have compared the tunneling current characteristics

of an array (collective) of clusters and of an isolated single cluster.

2. Experimental section

2.1 Materials and chemicals

1-hexyl-3-methylimidazolium tris(pentafluoroethyl)trifluorophosphate ($[C_6C_1Im][FEP]$) RTIL (high purity), and tetrabutylammonium hexafluorophosphate ($\geq 99.0\%$, electrochemical analysis) were purchased from Merck and Fluka respectively. The $[C_6C_1Im][FEP]$ mixed with molecular sieve was heated up at 85 °C under vacuum (10^{-6} mBar) overnight before use in order to remove the residue water. Sodium perchlorate ($>99\%$, anhydrous) and acetonitrile ($\geq 99.8\%$, anhydrous) were purchased from Alfa Aesar and Aldrich, respectively. BTPPA-TPFB was synthesized by metathesis of BTPPA-Cl and LiTPFB in 2 : 1 mixtures of methanol and water⁴⁸. Water with the resistivity of 18.2 M Ω .cm was prepared by a Millipore purification system.

Ligand synthesis: 4-(pyridin-4'-yl)benzenethiol was synthesized according to literature^{49, 50} with minor modifications. A detailed protocol is available in the electronic supporting information (ESI). In short, 4-Bromopyridine hydrochloride and 4-(methylthio)phenylboronic acid were coupled in a Suzuki reaction providing the methyl protected ligand. Subsequent treatment with an alkyl-thiolate resulted in the deprotected 4-(pyridin-4'-yl)benzenethiol, which oxidized in the presence of oxygen to 1,2-bis(4'-(pyridin-4''-yl)-phenyl)disulfane.

2.2 Synthesis of mixed monolayer protected Au₁₄₄ clusters

The synthesis of Au MPC was carried out under air atmosphere. HAuCl₄ (0.36 mmol, 1 eq) and TOABr (0.38 mmol, 1.1 eq) were added to a round bottom flask and dissolved in methanol (10 mL). After stirring for 5 min., the solution color had changed from yellow to red. Then 1,2-bis(4'-(pyridin-4''-yl)phenyl)disulfane (0.19 mmol, 0.53 eq.) dissolved in MeOH (5 mL) was added to the stirred solution and cooled to 0 °C. This mixture was stirred for 10 min. before 1-hexanethiol (1.53 mmol, 4.24 eq.) was added, followed by the immediately addition of a freshly prepared NaBH₄ solution (3.6 mmol, 10 eq. in 2 mL NanoPure water). The solution turned immediately black, indicating the formation of gold particles. After stirring for 1 h, the mixture was allowed to warm up to room temperature and stirred for another 3 hours at that temperature. The black NP were collected and centrifuged at 4000 rpm for 10 min. The supernatant was discarded and the pellet was washed 3 more times with fresh methanol to wash off the excess of organic molecules.

The formed particles were separated by their different solubility. The Au NP-mixture was suspended in acetone and centrifuged for 10 min. at 4000 rpm. Small Au clusters remained in solution whereas Au₁₄₄ MPCs precipitated and could be separated from bigger particles and gold-thiol-polymer with dichloromethane as solvent. The yield of Au₁₄₄ MPC was 5-10% with respect to the gold salt starting material. The clusters were analyzed by transmission electron microscopy (TEM), MALDI-ToF mass spectrometry, elemental analysis (EA) and thermogravimetric analysis (TGA). TEM pictures displayed Au particles with diameters of 1.7 ± 0.6 nm and MALDI-ToF MS displayed a broad peak between 30 000 and 34 000 amu which are both in agreement with reported values for hexylthiol stabilized Au₁₄₄ particles. As only the pyridyl-functionalized ligand comprises a N atom, the ratio between both ligands was calculated to be 10/1 from the weight percent of N (0.32) and C (17.82) obtained by EA. The TGA experiment displays the loss of 22.38 weight % attributed to the mass of the organic coating. These numbers are

in agreement with the composition of a hypothetical average particle as Au₁₄₄(SC₆H₁₃)₆₀(SC₆H₄C₅NH₄)₆.

2.3 Self-assembly

The Au₁₄₄(C₆S)₆₀(C₁₁H₈NS)₆ MPCs (m = 2.1 mg, M = 36 520 g/mol, n = 57 nmol) were dissolved in CH₂Cl₂ (3 mL), forming a solution with the concentration of 19 μ M. The hanging-meniscus type Pt(111) electrode was flame-annealed with butane flame (red heat, one minute) and subsequently cooled down in two different ways: (1) under dry Ar stream for about 10 min and (2) cooling in a closed flask containing water-saturated mixture of Ar/H₂ (4:1 v/v). After that, the electrode was immersed into the above cluster solution for 1 hour and rinsed by 10 ml of CH₂Cl₂ to remove all physisorbed MPC layers. The electrode was then immediately transferred into the deaerated electrochemical cell.

2.4 Electrochemistry

All electrochemical measurements (DPV) were carried out with an Autolab PGSTAT system. High-purity Ar gas (99.999%) was used to deaerate the electrochemical cell both before and during the measurement. An aqueous solution of 0.1 M NaClO₄, acetonitrile containing 0.01 M BTAPPA-TPFB and $[C_6C_1Im][FEP]$ IL served as the electrolyte. Blank experiments (without Au₁₄₄ MPCs in the system) were carried out to confirm the absence of charging peaks. A Pt wire served as both counter (CE) and reference (RE) electrodes in all DPV measurements. All potential scales were calibrated with respect to Fc/Fc⁺ redox couple. Pulse width: 60 ms, pulse height: 50 mV, period: 200 ms. The scan-rate in all experiments was 20 mVs⁻¹.

2.5 STM and STS measurements

Ex-situ STM images of the Au₁₄₄ MPCs were obtained by a Nanoscope E (Digital Instrument, DI). STS experiments were performed using a PicoSPM (Molecular Imaging, MI) under electrochemical conditions. A gold oxide-covered gold and a platinum electrode served as the reference electrode in aqueous solution and RTIL, respectively, and a platinum wire was used as counter electrode for both electrolytes. STM tips were prepared from mechanically cut Pt-Ir wires (diameter 0.25 mm, 80:20%) coated by polyethylene. Since the quality of STM tip coating is crucial for successful STS measurements, a cyclic voltammetric investigation of the STM tip was performed in situ before carrying out a STS measurement. The recorded double layer current should be less than 1 pA. The setpoint of tunneling current ranges from 60 to 150 pA and the bias voltage varies from 50 to 100 mV for a typical STS measurements.

3. Results and discussion

3.1 Controlled assembly of Au₁₄₄ MPCs on Pt(111)

Self-assembly of Au MPCs on surfaces has mostly been based on the covalent Au-S interaction (α,ω -dithiols linking the Au MPC to the gold surface).⁵¹ However, disintegration of Au MPCs usually takes place on an Au substrate. This is most likely related to the large thermodynamic imbalance between the bulk gold and the nanometer size gold cluster, where the ligand on the gold surface loses the contact with the cluster and forms a new bond with the Au substrate. We therefore developed a more stable Au MPC/substrate system. Initial attempts profiting from Au clusters coated by macromolecules exposing an integer number of functional groups as coupling units failed.⁵²⁻⁵⁵ A more robust Pt(111) surface has been chosen as the substrate which is known to coordinate to the lone pair of the pyridine nitrogen. As Au MPCs interacting with the Pt(111) substrate, gold clusters of narrow dispersity which were stabilized by a mixture of two

ligands were synthesized and isolated (see “Experimental section”). In brief, the synthesized Au clusters comprise in average 144 Au atoms functionalized with about 6 ligands exposing a pyridyl anchor unit (4-(4'-pyridyl)-thiophenolates) in a compact stabilizing coating consisting of about 60 hexylthiolate groups. It is noteworthy that the ratios between Au atoms of the cluster core and both ligands are numbers obtained by analytical methods involving large amounts of Au MPCs. Therefore, the obtained ratios are averaged numbers representing the most prominent composition of Au MPCs (which is $\text{Au}_{144}(\text{SC}_6\text{H}_{13})_{60}(\text{SC}_4\text{H}_4\text{C}_5\text{NH}_4)_6$). Minor variations in the number of gold atoms forming the cluster core and the numbers of different ligands exposed are very likely. The coordinating interaction of the peripheral pyridine subunits of the Au MPC with the Pt(111) substrate are expected to immobilize the particle at the surface as sketched in **Fig. 1**, while the poor attraction of the Pt(111) with the Au cluster capturing thiolates guarantees the integrity of the Au MPC on the substrate. **Fig. 1** depicts the concept of an Au_{144} MPC adsorbed on a Pt(111) surface through Pt-N coordinative bonding. Here, we report for the first time a new approach to control the Au MPCs on well defined surfaces.

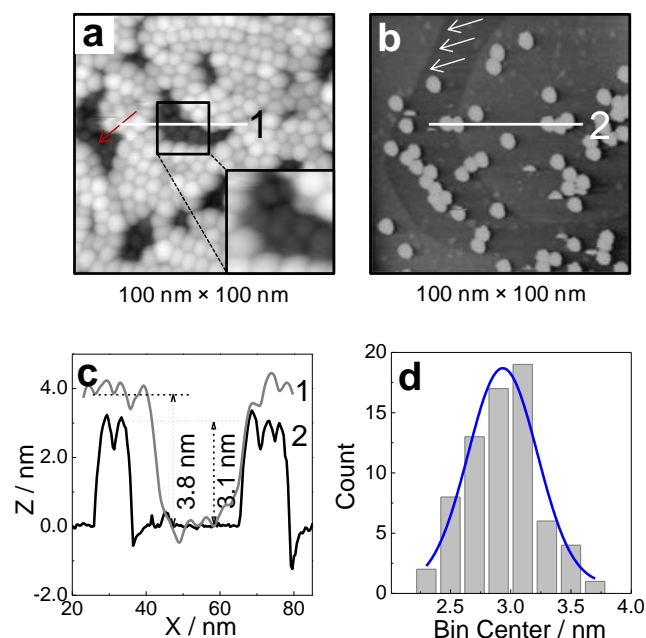


Fig. 2 (a, b) STM images of Au_{144} MPCs assembled on a Pt(111) surface after cooling down in pure Ar (a) and in a water-saturated H_2/Ar mixture (b). The inset picture, $19 \times 19 \text{ nm}^2$, in (a) shows an enlarged part of a “hole” in the top monolayer (marked with red arrows) displaying the nanoparticle assembly of the layer underneath. (c) Cross-section profiles from position 1 in (a) (grey profile) and 2 in (b) (black profile) as indicated by white lines. (d) Histogram of height distribution of individual clusters in (c).

Scanning tunneling microscopy (STM) was used to explore the surface morphology of Au_{144} MPCs on Pt(111). It was found that the morphology of Au_{144} MPCs on Pt(111) strongly depends on the pretreatment method of the Pt(111) substrate as well as on the concentration of Au_{144} MPCs in the solution for assembling. The clusters tend to form stacks of several densely packed monolayers with a hexagonally close-packed structure of each layer, if the Pt(111) surface has been cooled down in Ar atmosphere, as shown in **Fig. 2a**. The red arrows in **Fig. 2a** and the enlarged inset picture show the close-packed monolayer underneath the top layer. As it was not possible to determine the number of stacked monolayers in such a multilayer system, we just name this stacked multilayer system throughout this paper with the term “stacked monolayers”. However, cooling the Pt(111) surface in a

water saturated hydrogen/argon mixture (1:4) atmosphere led to the formation of a single sub-monolayer with individual clusters sparingly distributed on the surface (**Fig. 2b**). The atomic steps of the Pt(111) substrate are indicated by white arrows. **Fig. 2c** shows cross-section profiles of the white lines in **Fig. 2a** and **b**, revealing a typical monolayer height of 3.8 nm for the stacked monolayers, and 3.1 nm for the sub-monolayer, respectively. **Fig. 2d** shows the histogram of the height of Au_{144} MPCs constructed from more than one hundred individual clusters as shown in **Fig. 2b**, revealing a narrow distribution of height with the most probable value of 2.9 nm, which is very close to the theoretically predicted size of Au_{144} MPCs (3.2 nm, Au_{144} core + ligands). However, the measured diameter of each MPC (7.7 nm) is considerably larger than the theoretically predicted value. This discrepancy can be attributed to the convolution effect of the STM tip in X-Y direction. In addition, high resolution transmission electron microscopy (HR-TEM) was employed to determine the real average diameter of Au_{144} MPCs to be 1.7 nm, corresponding to the characteristic core size of Au_{144} MPCs. We already emphasize here that the narrow size distribution of Au_{144} MPCs plays an important role for obtaining reproducible data by single electron tunneling experiments on different clusters (see section 3.3).

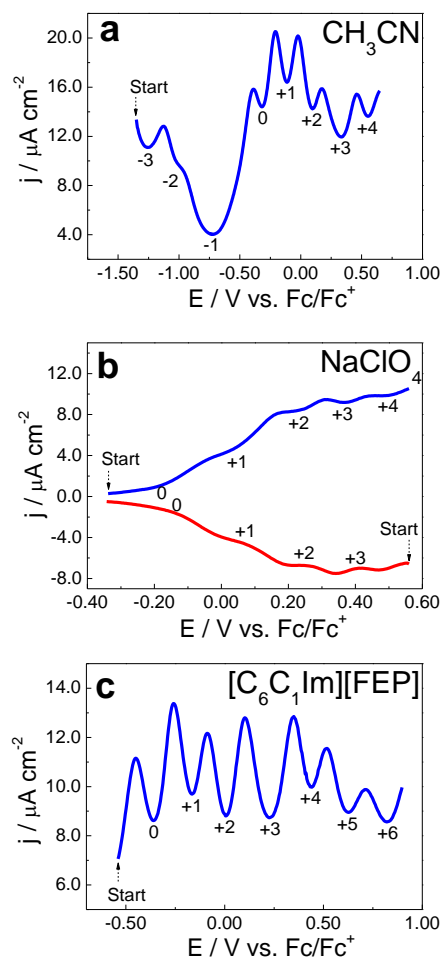


Fig. 3 Differential Pulse Voltammograms (DPV) of Au_{144} MPCs of a substrate with stacked monolayers on a Pt(111) electrode (as shown in **Fig. 2a**). (a) In 0.01 M BTTPA-TPFB/ CH_3CN , (b): In 0.1 M aqueous NaClO_4 , (c): in RTIL $[\text{C}_6\text{C}_1\text{Im}][\text{FEP}]$. Pulse width: 60 ms, pulse height: 50 mV, period: 200 ms, scan rate 20 mVs^{-1} .

The pronounced dependence of the surface morphology of Au_{144} MPCs on Pt(111) on the cooling conditions of the Pt(111) substrate could be due to the presence or absence of a water film on the Pt(111) surface under different atmospheric cooling

conditions. The water film is believed to exist on the Pt(111) surface if it is cooled down in a water-saturated Ar/H₂ mixture, which serves as an interface between the Pt(111) surface and the organic phase containing the dissolved Au₁₄₄ MPCs during assembling. Therefore, the Au₁₄₄ clusters diffusing towards the Pt(111) surface from the bulk of the solution must penetrate initially through this water film, which is energetically unfavorable considering the hydrophobic nature of the Au₁₄₄ MPCs ligand shell, and therefore prevents the formation of stacked monolayers. This condition was then further chosen as the typical method of sample preparation with the formation of a sub-monolayer, which plays an important role for the subsequent charge transport studies.

3.2 Electrochemical characterization of Au₁₄₄ MPC assemblies

Prior to investigating the electrical properties of Au MPCs immobilized on electrode surface, the electrochemical properties of Au₁₄₄ MPCs were first examined in the bulk phase of organic solution (0.1 M TBAPF₆/CH₃CN + Toluene) using the standard procedure of differential pulse voltammetry (DPV, Fig. S1 in the ESI). The DPV curve reveals a typical multiple quantized charging up to thirteen states with an average peak-to-peak spacing (ΔE , only considered as marked with asterisks) of 0.264 ± 0.02 V (Fig. S1), which confirms electrochemically the existence of Au MPCs of the expected size. The average cluster capacitance (C_{MPC}) corresponds to a value of 0.608 ± 0.05 aF derived from peak-to-peak potential spacing with the formula $C = e/\Delta E$. This multiple charging feature, as well as the assignment of charge states, fully agree with the data reported in the literature,^{56, 57} where Au₁₄₄ (C₆H₁₃S)₆₀ MPCs were employed.

Fig. 3a shows the anodic DPV scan obtained for a substrate with stacked monolayers of Au₁₄₄ MPCs on a Pt(111) electrode surface in deoxygenated acetonitrile containing 0.01 M BTPPA-TPFB as the supporting electrolyte. Six well-defined maxima are observed within the potential range between -1.50 and +1.0 V vs. Fc/Fc⁺. These maxima are attributed to the discrete charging of Au MPCs within the monolayer i.e. the electrochemical double layer charging.^{12, 31} The large wide gap at charge state -1 in Fig. 3a is due to the very large bulky size of both the cation and the anion of the supporting electrolyte, as described in the recent literature.⁵⁸ The average peak-to-peak spacing (ΔE , only considered from the 0 to +4 states) amounts to 0.188 ± 0.01 V, which translates itself into an average capacitance per cluster of 0.852 ± 0.04 aF.

The DPV of the substrate with Au₁₄₄ stacked monolayers in 0.1 M NaClO₄ (Fig. 3b) shows that only the positive charge states of the cluster were accessible. This observation is ascribed to ion-induced rectification⁵⁹ and ion-coupled electron transfer⁶⁰. I.e., the incorporation of ions into the cluster ligand shell controls the electron transfer between the MPC and the electrode, which in turn limits the accessibility of charge states in the DPV.⁶¹ In the present case, the Na⁺ cation cannot enter, whereas the ClO₄⁻ anion, due to its hydrophobic nature, can penetrate into the hydrophobic ligand shell leading to the absence of negative and the appearance of positive charge states in the DPV (Fig. 3b). This results in an average peak-to-peak spacing of 0.134 V corresponding to a capacitance value of 1.20 aF, which is close to the result reported in the literature.^{59, 62}

The same Au₁₄₄ MPCs stacked monolayer was further investigated in RTIL. The use of an ionic liquid as the electrolyte may enable to access more charging states due to the wide potential window. In addition it allows long-term stability by its unique property of non-volatility, which is highly required for the subsequent STS measurements. Fig. 3c shows the DPV of

stacked Au₁₄₄ MPCs monolayers on a Pt(111) surface in [C₆C₁Im][FEP] RTIL. Compared to the case of organic (Fig. 3a) and aqueous solvent (Fig. 3b), not only uniform charging states but also much more intensive DPV peak current signals were observed in the ionic liquid. These intense DPV current signals observed in IL may be attributed to the higher total ionic concentration and better incorporation of ions compared to the other two electrolytes.⁶³ An average peak-to-peak spacing of 0.194 ± 0.03 V was observed with a corresponding capacitance value of 0.84 ± 0.11 aF, which ranges between the value obtained for organic (CH₃CN) and aqueous solution. The different capacitance values for the same cluster in the different three electrolytes (Table 1 and Table S2) mainly arise from different ion permeability into the ligand shell and the different dielectric permeability of the solvents.^{61, 63, 64}

The assignment of the charge state of an immobilized stacked monolayer was done by the so-called immersion technique.^{58, 65} A selected example is demonstrated in the ionic liquid case in Fig. S2 of the ESI. A series of current transients against time due to double layer charging was recorded by changing the immersion potential. The charging current is either negative or positive (inset, Fig. S2), and varies systematically with the chosen immersion potential. A series of systematically recorded current transients is integrated at a fixed time scale (5 s after immersion) yielding a charge density which represents the consumed charge for building up the electrochemical double layer, and is plotted versus the immersion potential. The potential of zero-crossing represents an estimation of PZTC. The PZTC of Au₁₄₄ stacked monolayers in [C₆C₁Im][FEP] is -0.34 V vs. Fc/Fc⁺, which is close to the minimum of the DPV curve, as indicated in Fig. S2. As a consequence, the charge state of this minimum at -0.34 V is assigned to the zero charge state. These electrochemical studies show the multiple discrete states accessible in one single element at room temperature, which may enable an increased data storage density of such a prototype switch. Additionally, the strong dependence of the electrochemical characteristics of the MPCs on the chosen electrolyte shows that this system can be finely tuned to control each single electron transport event. These features make our MPCs versatile and appealing materials for molecular electronics applications. However, the electrochemical studies only give the overall current signal from assemblies. Indeed, for realizing the future nano/molecular electronics, it is necessary to understand the charge transport behavior of individual clusters by incorporating them in between two electrodes. Therefore, we use EC-STs for characterizing the electrical properties of individual clusters.

3.3 Scanning tunneling spectroscopy (STS) of single Au₁₄₄ MPCs

All STS experiments were done on the sample shown in Fig. 2b, since the surface contains both "stand-alone" and "grouped" Au₁₄₄ MPCs. For STS measurements, both types are available on one sample. Due to the fast evaporation of the organic solvent as well as the problem of the instability of STM tip coating, the STS measurements are limited to aqueous solution and ionic liquid.

In order to obtain reliable STS traces, the whole system requires an extremely high mechanical stability. In order to achieve this, the setup was at least stabilized for more than twelve hours prior to the experiment and the STS experiments were typically performed around midnight in order to minimize the disturbance from environments. To verify the stability of the setup practically, a small surface area of 20×20 nm² was repeatedly imaged and the stability was evaluated from the drift of the STM image. The STM tip was finally positioned on the

central top of one Au₁₄₄ MPC by gradually decreasing the scanning area if no obvious drift was observed (< 2 nm/image, Fig. S3 of the ESI). The tunneling current response was recorded at a constant position of the tip while simultaneously sweeping both, the substrate potential E_s and the tip potential E_t at a constant bias mode with the feedback loop disabled. In this case, each equilibrium redox charge state of the Au₁₄₄ MPCs comes into resonance while sweeping both, the Fermi levels of the substrate and the tip. The single electron transfer takes place from the Pt substrate to the STM tip, if a positive bias was applied, through the Au₁₄₄ MPCs via a two-step electron transfer mechanism, Fig. 4a.

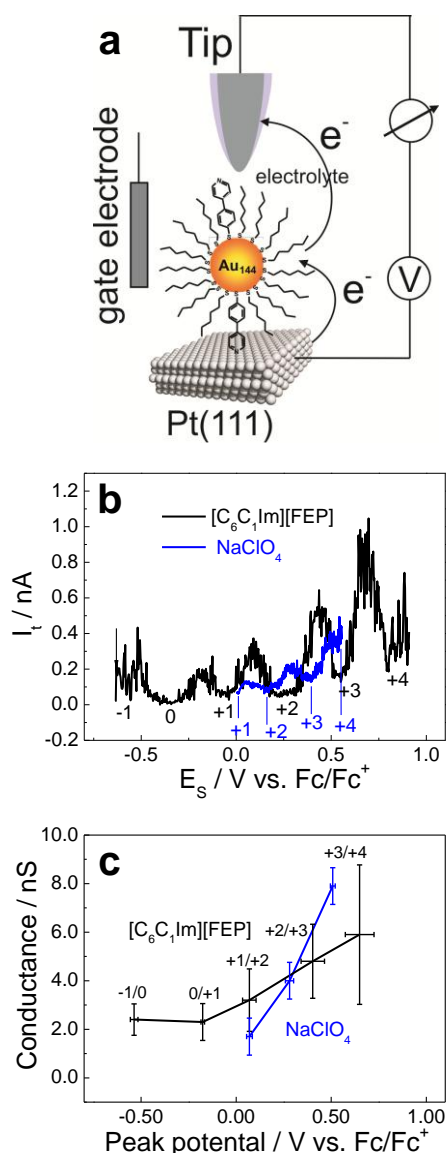


Fig. 4 (a) Schematic of scanning tunneling spectroscopy (STS). (b) Tunneling current response with respect to substrate potential on an individual well-separated Au₁₄₄ MPCs on Pt(111) surface. Black curve: in [C₆C₁Im][FEP] RTIL I_{set}: 50 pA, V_{bias} (E_{tip} - E_{substrate}): +0.1 V, sweep rate: 0.8 V s⁻¹. Blue curve: in 0.1 M NaClO₄ aqueous solution. I_{set}: 60 pA, V_{bias}: +0.05 V, sweep rate: 0.8 V s⁻¹. The numerical labels describe the charge state of Au₁₄₄ MPCs under different potentials. (c) A comparison of tunneling current peak intensities of an individual Au₁₄₄ MPCs in RTIL [C₆C₁Im][FEP] (black curve) with 0.1 M NaClO₄ aqueous solution (blue curve). The numerical labels describe the transition of the charge states that are associated with the peaks in Fig. 4b.

In order to avoid artifacts from the STS curves, a control experiment was firstly carried out with a redox inactive SAM of

1-undecanethiol on an Au(111) surface in 0.1 M HClO₄ (Fig. S6 of the ESI). Evidently no enhancement of the tunneling current was observed during the potential sweep, but only a stable background tunneling current of 0.1 nA. This result supports unambiguously that the enhancement of the tunneling current in Fig. 4b indeed originates from the existence of Au₁₄₄ MPCs trapped between the STM tip and the substrate.

Table 1. Comparison of the average peak potential spacing and single cluster capacitance values measured in various electrolytes by DPV and STS.

Electrolyte	Method	ΔE / V	C / aF
CH ₃ CN	DPV	0.188	0.852
NaClO ₄	DPV	0.134	1.198
	STS	0.219	0.730
[C ₆ C ₁ Im][FEP]	DPV	0.194	0.840
	STS	0.297	0.540

The blue curve in Fig. 4b shows a typical STS profile recorded in 0.1 M NaClO₄/H₂O with the tip on the top of an isolated Au₁₄₄ MPC. The peak position and the magnitude of the enhancement of tunneling current are found to be reproducible within several subsequent measurements on one cluster (Fig. S4 in the ESI). As displayed in Fig. S5 in the ESI, the peak positions of the charging current in the DPV studies are independent of the amount of clusters on the electrode surface. The assignment of the charge states in the tunneling current spectra was based on the potential scale of the DPV experiment, as indicated by the numerical labels in Fig. 4b. The average peak-to-peak spacing in the tunneling current traces amounts to 0.219 ± 0.01 V, corresponding to an average capacitance value of 0.730 aF, which is by ~ 40% smaller than the value determined by DPV (Table 1). This significant discrepancy of the capacitance value was also reported by Albrecht et. al,²⁶ where a very similar cluster of Au₁₄₅ (hexylmercaptane)₃₈(4-mercaptopyridine)₁₂ MPCs (abbreviated as Au₁₄₅(C₆S)₃₈(4MP)₁₂) was studied under electrochemical control (0.1 M KClO₄). The authors suggested that this discrepancy could be due to a smaller contribution of capacitance from the diffuse layer in the STS configuration compared to DPV, and a substrate-solution potential drop parameter (ξ).^{63, 66} In more details, the conductance of the tunneling current mainly happens through the minority ligand of 4-pyridylbenzene-1-thiol due to the coordinating bond between platinum and pyridyl. However, the capacitance measured by DPV is contributed collectively by the entire mixed monolayer, mainly from the majority ligand of hexane-1-thiol (90%). This explanation is further supported by the fact that a very close capacitance value (1.20 aF (ours) vs. 1.08 aF (ref. 26)) as determined by DPV was observed for both systems, since they bear the common dominant ligand, namely hexane-1-thiol. However, the capacitance value determined by STS in our case (0.73 aF) is by ~15% lower than that reported in the literature (0.86 aF),²⁶ indicating that STS is more sensitive to the local environment, i.e. the local dielectric constant (C = ε₀ε_rA/d), which highly depends on the nature of ligands.

STS was further applied to investigate the local electrical properties of individual Au₁₄₄ MPCs in [C₆C₁Im][FEP] RTIL. The potential of the STM tip was swept between -0.64 and 0.9 V by keeping a constant bias of 0.10 V. Fig. S7 in the ESI shows the highly reproducible STS traces obtained on one cluster, indicating the high stability of the tip-cluster-substrate junction. Moreover, we also conducted the STS measurements on different clusters, and a selection of representative traces from five different clusters are plotted together and shown in Fig. S8 of the

ESI. Evidently, the traces coincide well with little deviation, which demonstrates the reproducibility and reliability of our measurements. One typical STS curve was shown in the black curve in **Fig. 4b**. Compared to the case in aqueous solution (blue curve), the enhancement of tunneling current was observed in a wider potential window, however. The average peak-to-peak spacing amounts to 0.297 ± 0.02 V, corresponding to an average capacitance of 0.54 aF, which is by $\sim 40\%$ smaller than the value obtained from an ensemble of Au₁₄₄ MPCs by DPV (0.84 aF, **Table 1**). This trend in the ionic liquid is in accordance with that observed in aqueous electrolyte and can also be explained by the same mechanism of diffuse layer contribution.

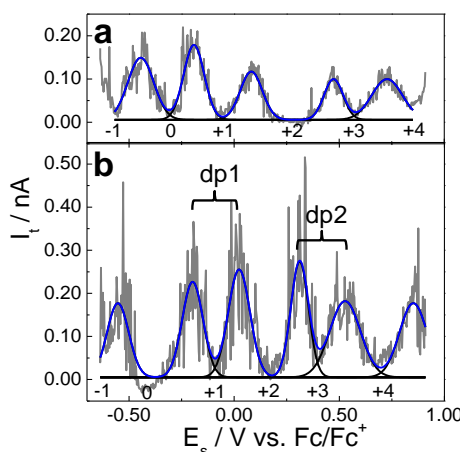


Fig. 5 Comparison of the STS response of Au₁₄₄ MPC in (a) densely packed monolayer and (b) well-separated individual ones in [C₆C₁Im][FEP] RTIL. I_{set} : 50 pA, V_{bias} : +0.1 V, sweep rate: 0.8 V s⁻¹.

The average tunnelling conductance values at each charge state are 1.7, 4.0, 7.9 and 2.4, 2.3, 3.2, 4.8, 5.9 nS in 0.1 M NaCO₄ and RTIL, respectively, and are plotted in **Fig. 4c**. The increase of tunneling current at more positively charged states was observed in both electrolytes, which strongly supports the qualitative explanation by Albrecht et al.,²⁶ who ascribed it to an increase of dielectric saturation i.e., the organisation of solvent molecules with increased charge state. As a result, a decrease of re-organisation energy of solvent molecules increases the tunneling rate values. Therefore, the dielectric saturation phenomenon is more predominant than the electronic coupling between clusters. However, we note that this monotonous increase of the tunneling current with increasing charge state was not always observed (see **Fig. 5**). This could be explained by either i) the high sensitivity of the tunneling current to the exact tip position relative to the Au₁₄₄ MPC surface; ii) fluctuations of the gap between STM tip and Au₁₄₄ MPC.

3.4 Comparison between single clusters and arrays of clusters: inter-particle interactions

The EC-STs data showed that the tunneling response depends strongly on the average distance between the particles. This was realized by comparing the STS results for individual but well-separated NPs with those of individual NPs in a close-packed monolayer domain of the same substrate. **Fig. 5** shows such a comparison recorded in [C₆C₁Im][FEP] RTIL. Au₁₄₄ MPCs in a close-packed environment (**Fig. 5a**) show no doublet peaks in their EC-STs traces, whereas the STS response of individual well-separated NPs (**Fig. 5b**) shows doublet peaks as indicated by dp1 and dp2.

The peak to peak spacing and the cluster capacitance for both close-packed and individual particles are shown in **Table S1** of

the ESI. For close packed particles (**Fig. 5a**), the peak to peak spacing is 0.25, 0.28, 0.39, 0.26 V, and for individual particles (**Fig. 5b**) 0.36, 0.22, 0.29, 0.21 and 0.32 V. The large gap in **Fig. 5a** corresponds to the gap observed at the charge state +3 in the DPV, which was induced by the ionic liquid electrolyte (**Fig. 3**). Each peak in dp1 and dp2 are separated by ~ 0.22 V, which is the Coulomb repulsion energy between the electrons (charging energy). The wide gap in-between the -1/0 and 0/+1 transition corresponds to the HOMO-LUMO gap of 0.14 V, indicating that the single Au₁₄₄ MPC has a molecular nature as opposed to the observation in array of clusters and ensembles measured by STS and DPV experiments (**Fig. 5a** and **Fig. 3c**). Recently, the discrete nature of electronic spectra was observed for Au₁₄₄ (C₆H₁₄)₆₀ ensemble clusters by lowering the temperature to 77 K.^{67, 68} Thus the disappearance of the HOMO-LUMO gap in the ensemble clusters at room temperature could arise from the Coulomb coupling between neighboring NPs. This clearly confirms that inter-particle interactions strongly influence the electrical properties and corresponding energy level spectra of Au MPCs and will have to be considered when using them as electronic elements in potential multistate electronic switches. These detailed studies reveal the potential of MPC based materials for future nano electronic devices. Engineering of the individual cluster materials into electronic circuits remains challenging however.

4. Conclusions

In conclusion, we demonstrate an increased control over both, the assembly and the electronic coupling of Au MPCs on an atomically flat electrode. By choosing Pt(111) as substrate and by synthesizing Au MPCs exposing a few pyridyl-groups coordinating to the substrate, the stability of the immobilized clusters is considerably improved. By varying the deposition conditions, samples coated with stacked layers consisting of closely packed Au MPCs or samples decorated with laterally separated individual Au MPCs are obtained. Electrochemical experiments were performed with samples ranging from dissolved Au MPCs in bulk solution, over stacked layers of Au MPCs down to single laterally separated Au MPCs. In all electrochemical experiments discrete charging events are resolved corroborating the narrow dispersity of the Au MPCs and demonstrating their potential as single electron switches. The spacing of the electrochemically addressed energy levels and thus also the capacity of the Au MPCs however, depends on the surrounding electrolyte. This was demonstrated for stacked layers of Au MPCs by DPV, and for individual immobilized Au MPCs by STS experiments. The latter studies also demonstrate that the energy level mapping of single Au MPC depends on the proximity of the neighboring clusters. The tunneling conductance increases and the HOMO-LUMO gap appears in the case of the isolated Au₁₄₄ clusters compared to the stacked array of clusters.

All together the lateral control of the Au MPC assembly provides samples fulfilling all requirements for room temperature single electron switches. In particular their multistate character observed in ionic liquids is appealing with respect to future applications. The single Au MPC tunneling characteristics (electron transport) depends on both, the composition of the surrounding electrolyte and the cluster arrangement. These aspects enhance the versatility of the system for molecular electronics applications and are the subject of current investigations. A possible combination of electrochemistry, STM/STS with other accessible single electron tunneling techniques, e.g. dynamic tunneling force microscopy (DTFM) should provide the power

for gaining new insight into the electronic and electron transport properties of many interesting nanoscale systems beyond our current understanding.⁶⁹

Acknowledgements

This research was supported by the National Research Program (NRP 62, project number 406240_126108) of the Swiss National Science Foundation (SNSF), other SNSF projects (200021_124643, 200020_144471 and 200020_140348), EC FP7 ITN “MOLESCO” project number 606728 and by the University of Bern and the University of Basel. The authors acknowledge the valuable scientific discussions with Dr. Wenjing Hong.

Notes and references

^a Freiestrasse 3, 3012 Bern, Switzerland. Fax: +41-(0)31-631-3993; Tel: +41-(0)31-631-4254; E-mail: fu@dcb.unibe.ch

^b St. Johannisring 19, 4056 Basel, Switzerland. Fax: +41-(0)61-267-1016; Tel: +41-(0)61-267-1006; E-mail: Marcel.Mayor@unibas.ch

^c P. O. Box 3640, 76021 Karlsruhe, Germany.

† Electronic Supplementary Information (ESI) available: See DOI: 10.1039/b000000x/

- W. Lu and C. M. Lieber, *Nat. Mater.*, 2007, 6, 841-850.
- S. Kubatkin, A. Danilov, M. Hjort, J. Cornil, J. L. Bredas, N. Stühr-Hansen, P. Hedegard and T. Bjornholm, *Nature*, 2003, 425, 698-701.
- E. Lortscher, J. W. Ciszek, J. Tour and H. Riel, *Small*, 2006, 2, 973-977.
- H. Song, M. A. Reed and T. Lee, *Advanced Materials*, 2011, 23, 1583-1608.
- J.-F. Dayen, E. Devid, M. V. Kamalakar, D. Golubev, C. Guédon, V. Faramarzi, B. Doudin and S. J. van der Molen, *Adv. Mater.*, 2013, 25, 400-404.
- A. M. Ionescu and H. Riel, *Nature*, 2011, 479, 329-337.
- S. W. Boettcher, N. C. Strandwitz, M. Schierhorn, N. Lock, M. C. Lonergan and G. D. Stucky, *Nat. Mater.*, 2007, 6, 592-596.
- W. Haiss, C. S. Wang, I. Grace, A. S. Batsanov, D. J. Schiffrin, S. J. Higgins, M. R. Bryce, C. J. Lambert and R. J. Nichols, *Nat. Mater.*, 2006, 5, 995-1002.
- J. C. Cuevas and E. Scheer, *Molecular Electronics: An Introduction to Theory and Experiment*, World Scientific, Singapore, 2010.
- H. Qian, M. Zhu, Z. Wu and R. Jin, *Acc. Chem. Res.*, 2012, 45, 1470-1479.
- S. Chen, R. S. Ingram, M. J. Hostetler, J. J. Pietron, R. W. Murray, T. G. Schaaff, J. T. Khoury, M. M. Alvarez and R. L. Whetten, *Science*, 1998, 280, 2098-2101.
- T. Laaksonen, V. Ruiz, P. Liljeroth and B. M. Quinn, *Chem. Soc. Rev.*, 2008, 37, 1836-1846.
- D. L. Klein, R. Roth, A. K. L. Lim, A. P. Alivisatos and P. L. McEuen, *Nature*, 1997, 389, 699-701.
- D. N. Weiss, X. Brokmann, L. E. Calvet, M. A. Kastner and M. G. Bawendi, *Appl. Phys. Lett.*, 2006, 88, 143507-143503.
- G. Schmid and U. Simon, *Chem. Commun.*, 2005, DOI: 10.1039/b411696h, 697-710.
- D. I. Gittins, D. Bethell, D. J. Schiffrin and R. J. Nichols, *Nature*, 2000, 408, 67-69.
- L. C. Brousseau, Q. Zhao, D. A. Shultz and D. L. Feldheim, *J. Am. Chem. Soc.*, 1998, 120, 7645-7646.
- E. Katz and I. Willner, *Angew. Chem. Int. Ed.*, 2004, 43, 6042-6108.
- M. Hesari, Z. Ding and M. S. Workentin, *Organometallics*, 2014, DOI: 10.1021/om500112j.
- D. L. Feldheim, K. C. Grabar, M. J. Natan and T. E. Mallouk, *J. Am. Chem. Soc.*, 1996, 118, 7640-7641.
- R. J. Tseng, C. Tsai, L. Ma, J. Ouyang, C. S. Ozkan and Y. Yang, *Nat Nano*, 2006, 1, 72-77.
- R. J. Tseng, J. Ouyang, C.-W. Chu, J. Huang and Y. Yang, *Appl. Phys. Lett.*, 2006, 88, 123506-123503.
- G. Schmid and B. Corain, *Eur. J. Inorg. Chem.*, 2003, 2003, 3081-3098.
- B. A. Korgel, *Nat. Mater.*, 2007, 6, 551-552.
- M. Homberger and U. Simon, *Philosophical Transactions of the Royal Society A: Mathematical, Physical and Engineering Sciences*, 2010, 368, 1405-1453.
- T. Albrecht, S. F. L. Mertens and J. Ulstrup, *J. Am. Chem. Soc.*, 2007, 129, 9162-9167.
- P. Yang, I. Arfaoui, T. Cren, N. Goubet and M.-P. Pileni, *Nano Lett.*, 2012, 12, 2051-2055.
- V. Torma, T. Reuter, O. Vidoni, M. Schumann, C. Radehaus and G. Schmid, *ChemPhysChem*, 2001, 2, 546-548.
- J.-P. Choi and R. W. Murray, *J. Am. Chem. Soc.*, 2006, 128, 10496-10502.
- D. Lee, R. L. Donkers, J. M. DeSimone and R. W. Murray, *J. Am. Chem. Soc.*, 2003, 125, 1182-1183.
- R. W. Murray, *Chemical Reviews (Washington, DC, United States)*, 2008, 108, 2688-2720.
- A. M. Ricci, E. J. Calvo, S. Martin and R. J. Nichols, *J. Am. Chem. Soc.*, 2009, 132, 2494-2495.
- P. Salvatore, A. Glargaard Hansen, K. Moth-Poulsen, T. Bjornholm, R. John Nichols and J. Ulstrup, *PCCP*, 2011, 13, 14394-14403.
- T. Albrecht, A. Guckian, J. Ulstrup and J. G. Vos, *Nanotechnology, IEEE Transactions on*, 2005, 4, 430-434.
- T. Albrecht, K. Moth-Poulsen, J. B. Christensen, J. Hjelm, T. Bjornholm and J. Ulstrup, *J. Am. Chem. Soc.*, 2006, 128, 6574-6575.
- T. Albrecht, K. Moth-Poulsen, J. B. Christensen, A. Guckian, T. Bjornholm, J. G. Vos and J. Ulstrup, *Faraday Discuss.*, 2006, 131, 265-279.
- N. J. Kay, S. J. Higgins, J. O. Jeppesen, E. Leary, J. Lycoops, J. Ulstrup and R. J. Nichols, *J. Am. Chem. Soc.*, 2012, 134, 16817-16826.
- P. Petrangolini, A. Alessandrini, M. L. Navacchia, M. L. Capobianco and P. Facci, *The Journal of Physical Chemistry C*, 2011, 115, 19971-19978.
- Z. Li, Y. Liu, S. F. L. Mertens, I. V. Pobelov and T. Wandlowski, *J. Am. Chem. Soc.*, 2010, 132, 8187-8193.
- A. Mishchenko, M. Abdualla, A. Rudnev, Y. Fu, A. R. Pike and T. Wandlowski, *Chem. Commun.*, 2011, 47, 9807-9809.
- I. V. Pobelov, Z. Li and T. Wandlowski, *J. Am. Chem. Soc.*, 2008, 130, 16045-16054.
- Pavel Moreno-García, Hennie Valkenier, Yongchun Fu, Ilya Pobelov, Wenjing Hong, Jan C. Hummelen and T. Wandlowski, 2014, In preparation.
- S. F. L. Mertens, K. Blech, A. S. Sologubenko, J. Mayer, U. Simon and T. Wandlowski, *Electrochim. Acta*, 2009, 54, 5006-5010.
- S. F. L. Mertens, G. Meszaros and T. Wandlowski, *Phys. Chem. Chem. Phys.*, 2010, 12, 5417-5424.
- D. Steiner, A. Aharoni, U. Banin and O. Millo, *Nano Lett.*, 2006, 6, 2201-2205.
- P. Liljeroth, K. Overgaard, A. Urbietta, B. Grandidier, S. G. Hickey and D. Vanmaekelbergh, *Phys. Rev. Lett.*, 2006, 97, 096803.
- M. A. Mezour, I. I. Perepichka, J. Zhu, R. B. Lennox and D. F. Perepichka, *ACS Nano*, 2014, 8, 2214-2222.
- D. J. Fernán, H. Dung Duong, Z. Ding, o. Brevet and H. H. Girault, *PCCP*, 1999, 1, 1461-1467.
- A. Gallardo-Godoy, M. I. Torres-Altora, K. J. White, E. L. Barker and D. E. Nichols, *Bioorg. Med. Chem.*, 2007, 15, 305-311.
- H. Qian and R. Jin, *Chem. Mater.*, 2011, 23, 2209-2217.
- S. Chen, *The Journal of Physical Chemistry B*, 2000, 104, 663-667.
- T. Peterle, A. Leifert, J. Timper, A. Sologubenko, U. Simon and M. Mayor, *Chemical Communications*, 2008, DOI: 10.1039/B802460J, 3438-3440.
- T. Peterle, P. Ringler and M. Mayor, *Adv. Funct. Mater.*, 2009, 19, 3497-3506.
- J. P. Hermes, F. Sander, T. Peterle, R. Urbani, T. Pfohl, D. Thompson and M. Mayor, *Chemistry – A European Journal*, 2011, 17, 13473-13481.
- J. P. Hermes, F. Sander, U. Fluch, T. Peterle, D. Thompson, R. Urbani, T. Pfohl and M. Mayor, *J. Am. Chem. Soc.*, 2012, 134, 14674-14677.
- B. M. Quinn, P. Liljeroth, V. Ruiz, T. Laaksonen and K. Kontturi, *J. Am. Chem. Soc.*, 2003, 125, 6644-6645.
- J. F. Hicks, D. T. Miles and R. W. Murray, *J. Am. Chem. Soc.*, 2002, 124, 13322-13328.
- K. Cui, S. De Feyter and S. F. L. Mertens, *Electrochem. Commun.*, 2012, 25, 128-131.
- S. Chen and R. Pei, *J. Am. Chem. Soc.*, 2001, 123, 10607-10615.
- W. Li, D. Wang, Q. Sun and B. Su, *Electrochem. Commun.*, 2011, 13, 875-878.

-
61. T. Laaksonen, O. Pelliniemi and B. M. Quinn, *J. Am. Chem. Soc.*, 2006, 128, 14341-14346.
 62. S. Chen, *J. Am. Chem. Soc.*, 2000, 122, 7420-7421.
 63. R. Guo, D. Georganopoulou, S. W. Feldberg, R. Donkers and R. W. Murray, *Anal. Chem.*, 2005, 77, 2662-2669.
 - 5 64. B. Su, M. Zhang, Y. Shao and H. H. Girault, *The Journal of Physical Chemistry B*, 2006, 110, 21460-21466.
 65. U. W. Hamm, D. Kramer, R. S. Zhai and D. M. Kolb, *J. Electroanal. Chem.*, 1996, 414, 85-89.
 - 10 66. A. M. Kuznetsov and J. Ulstrup, *The Journal of Physical Chemistry A*, 2000, 104, 11531-11540.
 67. H. C. Weissker, H. B. Escobar, V. D. Thanthirige, K. Kwak, D. Lee, G. Ramakrishna, R. L. Whetten and X. Lopez-Lozano, *Nat Commun*, 2014, 5, 3785.
 - 15 68. J. Koivisto, S. Malola, C. Kumara, A. Dass, H. Häkkinen and M. Pettersson, *The Journal of Physical Chemistry Letters*, 2012, 3, 3076-3080.
 69. N. Zheng, J. P. Johnson, C. C. Williams and G. Wang, *Nanotechnology*, 2010, 21, 295708.

20